Arrays of Parallel Connected Coaxial Multiwall-Carbon-Nanotube–Amorphous-Silicon Solar Cells

By *Hang Zhou,* Alan Colli, Arman Ahnood, Yang Yang, Nalin Rupesinghe, Tim Butler, Ibraheem Haneef, Pritesh Hiralal, Arokia Nathan,* and *Gehan A. J. Amaratunga**

Many nanotechnology-based enhancements for solar cells have been proposed.[1] On the one hand, inorganic nanoparticles, nanorods, and nanowires (NWs) have been incorporated into organic solar cells[2–7] to extend the available interface for charge separation and improve the overall mobility of the material. On the other hand, for conventional inorganic solar cells, it has also been theoretically shown that NW-like structures could potentially lead to a better collection efficiency of photogenerated carriers together with greater optical absorption from low-purity material.[8,9] Particular attention has been placed on the coaxial core/shell NW structure, where charge separation of photogenerated carriers occurs in the radial direction, that is, orthogonally to the optical absorption path. This idea can be implemented either with a core/shell NW p–n junction[10] or with a core/shell structure formed by two materials with type-II band alignment, which separate charge at the interface without the need for doping.[11,12] From a practical point of view, however, clear evidence of NW solar cells outperforming existing solutions based on planar thin films is still lacking.

Silicon-based solar cells currently dominate the photovoltaic (PV) market.[13] Several attempts have been made to fabricate solar cells based on coaxial silicon nanowires (SiNWs).[14,15] The efficiency of SiNW p–n and p–i–n junctions as nanoelectronic power sources has been measured down to the individual-NW level.[10,16] The interpenetrated p–n junction geometry based on coaxial NWs, however, still relies on carrier-collection paths composed of semiconductor materials, which pose constraints on collection efficiency due to path resistance.

Here, we extend this approach by fabricating solar cells with interpenetrated electrodes, that is, a multishell coaxial NW structure where a metallic inner core and a metallic outer shell act as proximity electrodes for the radial junction sandwiched in between. Specifically, our strategy is based on coating vertically aligned multiwall carbon nanotubes (MWNTs) with amorphous-silicon (a-Si:H) shells and indium tin oxide (ITO). MWNTs are known as quantum resistors, whose conductance is independent of the diameter and length of the tube (one unit of the conductance quantum $G_o = 2e^2/h = (12.9k\Omega)^{-1}$).[17] The use of MWNTs as core contacts can avoid electrical losses that might occur in other types of nanowires. Moreover, nanotube/nanowire (NT/NW) arrays form a natural light-trapping structure.[18] Indeed, a 25% increase of the short-circuit current is achieved for the NT/NW array compared to the planar a-Si cell used as reference. Most of this enhancement is measured to come from red photons. A similar experiment was recently carried out by Camacho et al., who used MWNTs as scaffold to support a CdTe heterojunction.[19] In contrast, our study concentrates on a-Si:H as a cheap and environment-friendly material, which at present is widely used in commercial solar-cell manufacturing. We also see that a-Si:H provides a more conformal coating on MWNTs compared to CdTe.

Figure 1a outlines the fabrication process of the coaxial MWNT/a-Si:H solar-cell devices (I-III) and their final physical structure (IV). Details of the fabrication process can be found in the Experimental section. Scanning electron microscopy (SEM) images of vertically aligned MWNTs arrays and of coaxial MWNT–amorphous-silicon structures are shown in Figure 1b. MWNTs are conformally coated with a-Si:H with no evident tapering. The solar cells exhibit a periodic 3D nanostructure, leading to an amplification of the effective cell area. From top to bottom, our solar cells comprise layers of ITO/intrinsic a-Si:H/n-type a-Si:H/MWNTs on a tungsten substrate. The solar cells are thus Schottky-type, as Schottky junctions are formed at the ITO/a-Si:H interface. The built-in electric field across the absorbing layer – intrinsic a-Si:H – is formed through the alignment of the Fermi levels between the n + doped a-Si:H and the ITO. The nominal band diagram for the structure is shown in Figure 1c. The work-function of the ITO is taken to be 4.9 eV. The band gap and electron affinity of a-Si:H are taken as 1.6 eV and 3.7 eV, respectively. The n-type amorphous Si is taken as having a Fermi level 0.2 eV below the effective conduction-band edge. The ITO and a-Si:H form a Schottky junction that is suitable for photogenerated hole flow.

In order to assess the performance of the coaxial MWNT/a-Si:H solar cells, a planar cell without MWNTs was prepared as a reference using the same fabrication process. The line-pattern

[*] Prof. G. A. J. Amaratunga, H. Zhou, Y. Yang, Dr. N. Rupesinghe, T. Butler, I. Haneef, P. Hiralal
Electrical Engineering Division
Department of Engineering
University of Cambridge
9 JJ Thomson Avenue, Cambridge CB3 0FA (UK)
E-mail: hz239@cam.ac.uk; gaja1@cam.ac.uk
Dr. A. Colli
Nokia Research Centre Cambridge U.K.
C/O Nanoscience Centre
Cambridge CB3 0FF (UK)
A. Ahnood, Prof. A. Nathan
London Centre for Nanotechnology
University College London
17-19 Gordon Street, London WC1H 0AH (UK)

DOI: 10.1002/adma.200901094

© 2009 WILEY-VCH Verlag GmbH & Co. KGaA, Weinheim

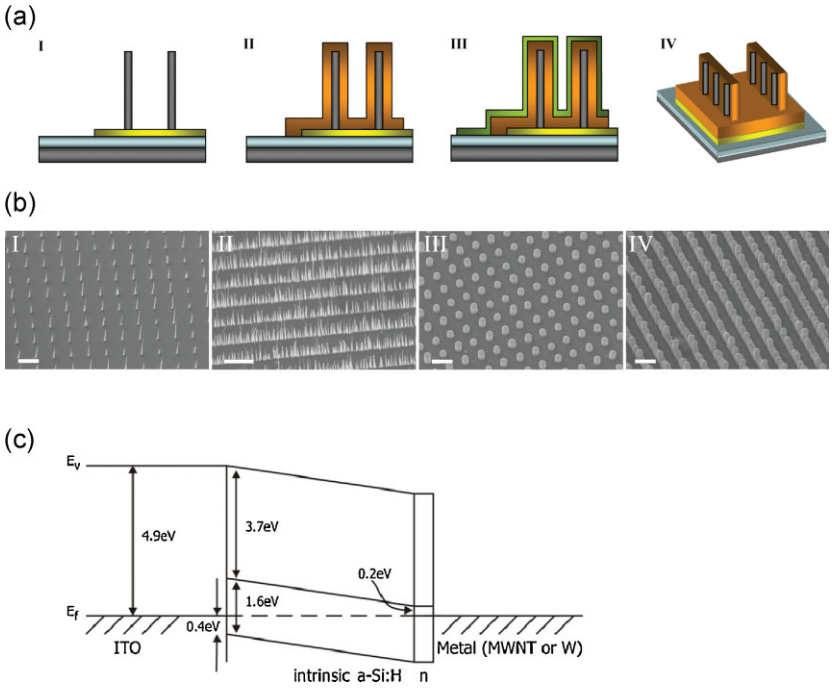

Figure 1. Schematics of device fabrication and SEM images of coaxial MWNT–amorphous-silicon solar-cell arrays. a) Device-fabrication processes: I) growth of patterned MWNTs on tungsten-coated (yellow layer) silicon wafer; II) deposition of amorphous silicon onto MWNTs arrays; III) deposition of transparent conductive top electrode (ITO, green layer); IV) schematic of a line-pattern array of coaxial MWNTs-amorphous silicon NWs; b) Tilted SEM images of MWNTs arrays in I) dot-pattern and II) line-pattern configurations as grown on tungsten; III) and IV) MWNTs arrays shown in I) and II), respectively, after a-Si:H coating. Scale bars = 2 μm. c) Band diagram of the ITO–amorphous-silicon Schottky diode.

geometry illustrated in Figure 1b IV, was used as the preferred configuration, as it has the advantage of packing the MWNT/NW structures with maximum density in one direction, while leaving a controllable air gap for light trapping. Hereafter, the device with line-patterned coaxial MWNT/a-Si:H arrays (Fig. 1b IV) is labeled as PV-1, and the planar reference device as PV-2. Both devices were fabricated on tungsten-coated SiO_2 substrates, and for both devices the thickness of the intrinsic a-Si:H is 500 nm on the planar parts of the cell. The a-Si:H thickness on the MWNTs is reduced to 200–300 nm in the plasma-enhanced chemical vapor deposition (PECVD) process. Device PV-1 has line-pattern arrays with a pitch of 2 μm. The average MWNT height is ~2.5 μm, and the overall diameter of the MWNT/a-Si:H/ITO multishell structure is ~640 nm. Both devices were tested under the same environmental conditions.

As PV-1 has nanostructures that enhance the surface area, a parameter defined as apparent current density is introduced to compare the performance of the two devices (see Experimental). The current–voltage characteristics of both PV-1 and PV-2 under AM1.5 are plotted in Figure 2. As shown in the figure, the short-circuit current densities of PV-1 and PV-2 are 7.04 mA cm^{-2} and 5.64 mA cm^{-2}, respectively. A short-circuit-current gain of ~25% is achieved in the coaxial structure over its planar counterpart. The open-circuit voltage is slightly improved in PV-1, about 27 mV larger than that of PV-2. The fact that the open-circuit voltage does not degrade over that of the planar cell clearly suggests that each coaxial MWNT/a-Si:H subcell has the same junction properties and does not 'work against' each other in terms of potential. The measured open circuit of 280 mV can be understood from the nominal band diagram in Figure 1c. Photogenerated holes will be collected in the ITO side of the ITO/i-a-Si:H Schottky barrier. This will continue until the Fermi level in the ITO is below the valence-band edge of the intrinsic a-Si:H. After this, no holes will flow into the ITO, as a barrier appears for hole flow. Hence, the effective open-circuit voltage is the separation between the ITO Fermi level and the valence-band edge of the intrinsic a-Si:H. In the nominal band diagram, this is 0.4 eV, close to the ~0.3 eV seen experimentally. Given that the open-circuit voltage is very close for both PV-1 and PV-2, it seems independent of the back contact, either MWNT or W. From semi-log plots of the dark $|I|$–V curves (Fig. 2b) we obtained an ideality factor of 3.72 for PV-1 and 5.7 for PV-2. The improvement in ideality factor in the array-structure case of PV-1 is ascribed to the thinner active i-a-Si:H layer (200–300 nm) compared to that in the planar PV-2 cell (500 nm), leading to a larger charge-separation field, and consequently less recombination in the active layer. The results indicate that the coaxial MWNT/a-Si:H array functions as thousands of individual free-standing photovoltaic NWs connected in parallel. The 25% increase in short-circuit current can be initially viewed as an enhancement of the effective cell area by 25% through the use of the MWNT array, that is, the array structure acting to 'concentrate the electrode area' of the cell. However, the change in the light-absorption properties of the array also have to be taken into account, as discussed below. The relative increase in efficiency of the MWNT/a-Si:H cell is also ~25%. In the following, we discuss our findings and investigate the merits of the cell geometry.

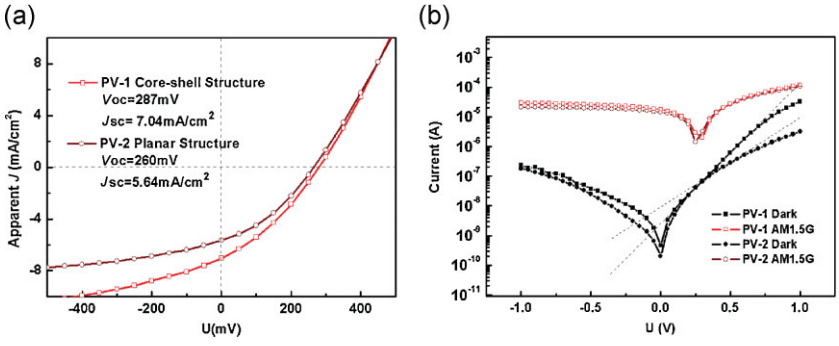

Figure 2. a) Current–voltage characteristics of a coaxial MWNT–amorphous-silicon solar cell (PV-1) and a planar solar cell (PV-2). b) Semi-log plot of current–voltage characteristic for PV-1 and PV-2.

WILEY InterScience DISCOVER SOMETHING GREAT
© 2009 WILEY-VCH Verlag GmbH & Co. KGaA, Weinheim

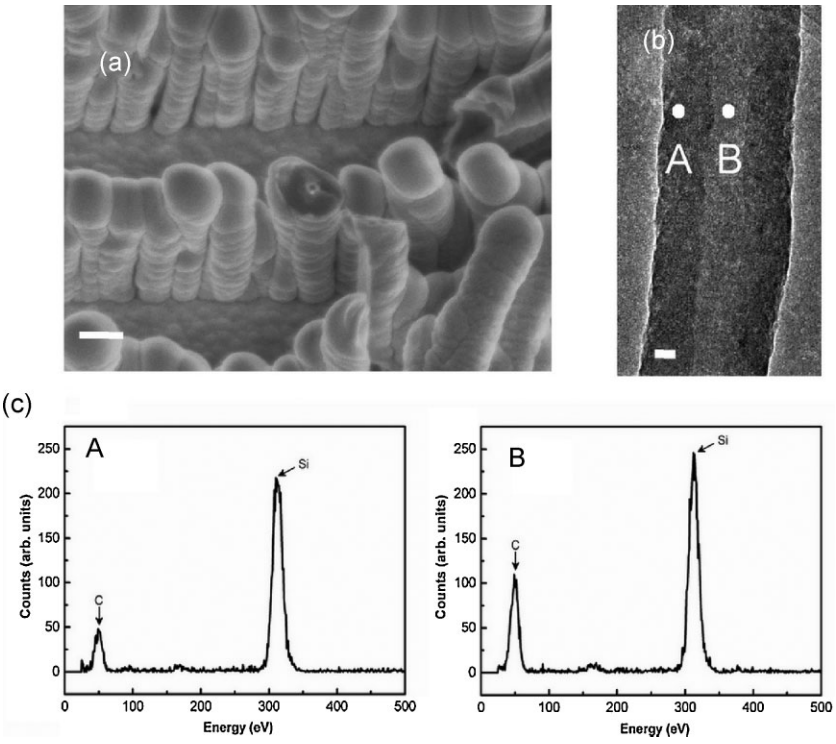

Figure 3. a) SEM image of a tip open coaxial MWNT–amorphous-silicon solar cell, showing the inner MWNTs, the a-Si:H photoabsorbing layer, and the outer ITO shell. Scale bar = 500 nm. b) TEM image of an a-Si:H-coated MWNT. Scale bar = 20 nm. c) EDX analysis performed on spot A (the shell) and B (the core) of the TEM image.

First, it is essential that MWNTs withstand the plasma-based deposition process for a-Si:H to serve as conductive paths for electron transportation. To verify this point, an SEM image of a coaxial wire with an open tip is shown (Fig. 3a, structure in the center). The MWNT inner core is still visible after a-Si:H deposition. A separate coaxial MWNT–amorphous-silicon NW sample was prepared for transmission electron microscopy (TEM) investigations. A TEM image is shown in Figure 3b with the corresponding energy-dispersive X-ray spectroscopy (EDX) analysis, showing the significantly higher carbon content of the core (Fig. 3c). The high conductivity of MWNTs as core electrodes can be inferred from the fact that the fill factor of device PV-1 in Figure 2a does not decrease compared to the reference cell PV-2.

The capacitances of these solar cells were also measured in order to determine whether or not the MWNTs are serving an active role in collecting currents. The capacitance for PV-1 measured at 0 V is 400 pF, which is 125 pF larger than that of PV-2 (275 pF). The 125 pF increment is mainly due to the effective-area enhancement realized through parallel connection of cylindrical capacitors forming the MWNT/a-Si:H/ITO array. A cylindrical capacitor model[20] was used to calculate the theoretical increment (see Experimental section). Assuming an average cylinder height of 2.5 μm, the calculated capacitance of one MWNT/a-Si:H/ITO cylinder would be 0.812 fF. Consequently, the total capacitance of the cylindrical nanocapacitor array (made of ~180 000 units) would be 146.16 pF, which is very close to the experimental difference of 125 pF between PV-1 and PV-2.

Efficiency of a-Si:H thin-film solar cells can be enhanced by effective light trapping, especially in the red spectral region, where absorption is weak.[21] The absorption curve for a-Si:H (optical bandgap ~1.7 eV) tails off in this region. For wavelengths between 600 and 700 nm, the absorption coefficients are in the $10^3\,cm^{-1}$ range.[22] Consequently, several micrometers of a-Si:H film are needed for full absorption of light at these wavelengths. However, a layer of a-Si:H with a thickness over 600 nm is not desirable, as a-Si:H layers exhibit the well-known Steabler–Wronski Effect (SWE) instability.[23] The defect density of a-Si:H increases with light exposure, therefore an increase in thickness leads to higher carrier recombination in the bulk absorption layer, lowering the solar-cell energy-conversion efficiency with time. Additionally, a thicker undoped absorption layer increases the series resistance for charge separation, and is seen as a loss of fill factor. One practical approach to circumvent these problems is to apply a higher electric field in thinner a-Si:H layers.[24] It is thus necessary to design an efficient light-trapping solution that allows the cell to fully absorb light even when its thickness is much less than the absorption length for light of a given wavelength. In the experimental devices, the typical a-Si:H layer thickness, which conformally covers the MWNT, is 200–300 nm thick.

Figure 4 illustrates the light trapping model implemented in the array of coaxial MWNTs/a-Si:H solar cells. Coaxial solar-cell arrays depicted in Figure 4a offer two distinct optical advantages over a conventional thin-film structure. First, incident photons that are normal to the device surface have a longer path along the axial direction of the coaxial columns, and therefore have a greater probability of being absorbed. Second, light incident over a certain range of angles can see multiple reflections from the sidewalls of these columns. The outcome is a natural light-trapping structure that can reduce the reflection over a broad spectrum. For planar cells, an antireflection coating is required to reduce reflection and achieve good optical confinement, but this solution only ensures antireflection over a narrow spectrum.

Blue and red color filters were added to the solar simulator in order to compare the short-circuit-current contribution from different spectral regions. Significant short-circuit-current enhancement appears in device PV-1 when the red filter is used

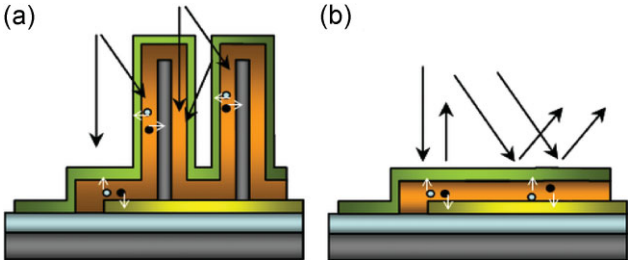

Figure 4. Schematic diagrams that compare the light-trapping structure and the charge-carrier collection direction of a) PV-1 and b) PV-2.

© 2009 WILEY-VCH Verlag GmbH & Co. KGaA, Weinheim

(Fig. 5a). The short-circuit current in this spectral region is about 1.4 times larger than that of PV-2 (Fig. 5b). On the other hand, the short-circuit current for PV-1 and PV-2 are closer in value when the blue filter is used. This suggests that longer wavelengths are more efficiently scattered by the 2-μm-pitch line pattern in the NT/NW array. It should be noted that though each MWNT/a-Si:H cell in a line may physically touch each other, without an air region between them, as shown in Figure 3a, what matters optically is the pitch/separation between the metallic MWNTs, as the ITO and a-Si:H layers are optically transparent. Further investigations are under way to optimize the pitch that would allow the maximum nanostructure density, while ensuring the best wavelength-dependent light-trapping properties (including line patterns with variable spacing). Figure 5c shows the external quantum efficiency (EQE) for both core/shell (PV-1) and planar (PV-2) structure devices. PV-1 demonstrates its superior light-trapping properties over PV-2 by producing a larger EQE in the wavelength region between 570 nm and 760 nm.

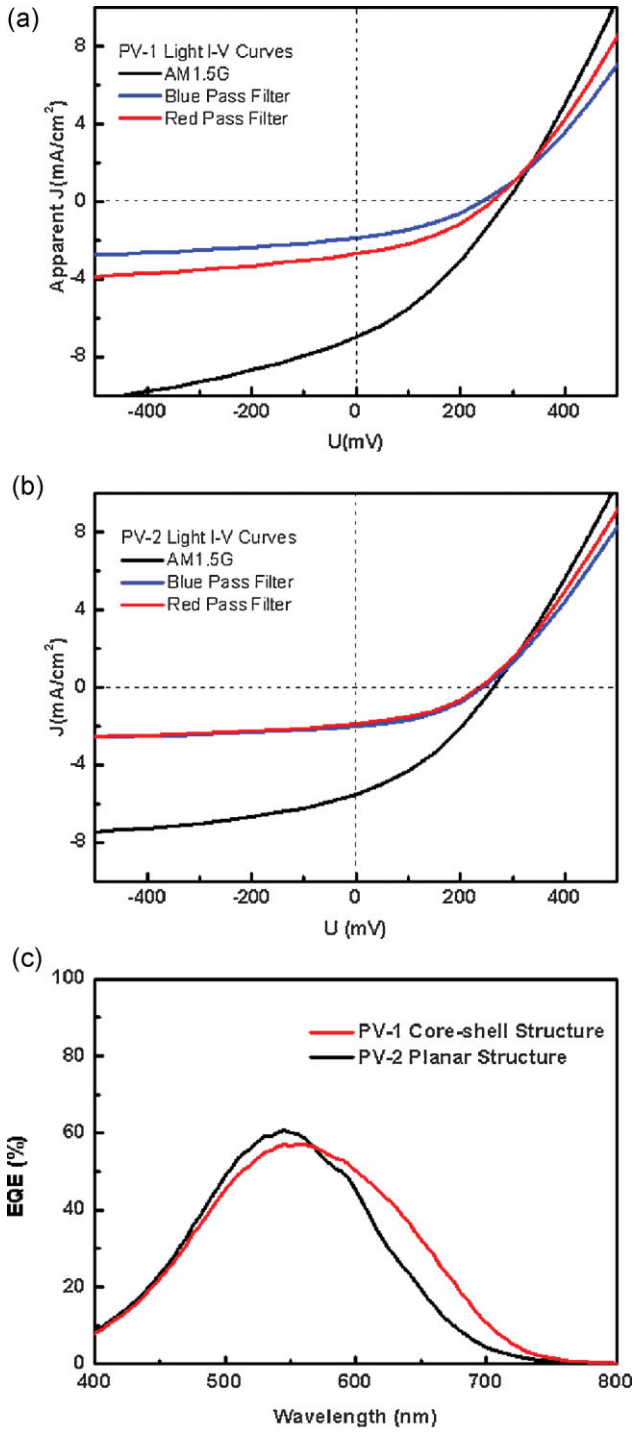

Figure 5. a,b) Plots of current–voltage characteristics for PV-1 and PV-2 under color-filtered illumination and EQE curves. c) EQE of device PV-1 and PV-2.

Finally, there must be another electrical merit that leads to a better diode ideality factor. We attribute this to the vertical structure of MWNTs, which leads to the orthogonalization of the direction of light absorption and charge-carrier transport. For the planar solar-cell structure (Fig. 4b), there are more charge carriers generated on the illuminated side of the cell when the light hits the surface. One species of photogenerated carriers (electrons in our case) will therefore have a longer path to travel than the other before collection by the electrode. Conversely, in the radial junction structure (Fig. 4a), while light is being absorbed along the axial direction, both electrons and holes are moving radially, and on average cover an equal distance to reach the metallic junction before charge collection.[1,8] The final outcome is that the average carrier-drift time of a particular type is shortened, and the chance for electron–hole recombination in the absorption region is reduced, leading to a better diode ideality factor.

In summary, we report coaxial solar cells realized using carbon nanotubes as the core electrode. Arrays of coaxial multi-wall-carbon-nanotube–amorphous-silicon solar cells are fabricated and characterized. A short-circuit-current enhancement of ~25% has been achieved over the conventional planar structure, owing to the highly effective light-trapping structure of the coaxial MWNT/a-Si:H nanowire array. Our findings suggest that solar cells with higher efficiency can be fabricated in a similar way on MWNT electrodes using many other low-cost thin-film materials.

Experimental

Device Fabrication: The fabrication process of our solar-cell device started with the sputtering of a thin tungsten layer (80 nm) onto a Si/SiO_2 insulating substrate as the bottom contact. Nickel, used as catalyst to grow MWNTs, was then deposited onto the tungsten via e-beam lithography patterning. The pattern can be designed in such a way that only a single standing carbon nanotube is grown on each catalyst site [25–27]. Vertically aligned MWNTs were grown using a direct-current (DC) PECVD method. In device PV-1, a line array of MWNTs with 239 rows and 2-μm pitch was grown. The tungsten layer, together with the as-grown MWNTs, served as the back electrode for the device. To continue the solar-cell-fabrication process, n-type (~25 nm) and intrinsic a-Si:H (~500 nm) layers were sequentially deposited onto this back electrode by radio-frequency PECVD (Fig. 1a II), and a 60 nm ITO film was finally deposited onto the intrinsic a-Si:H layer as the front contact (Fig. 1a III). The whole solar-cell area is defined by the bottom tungsten layer, which is about 0.5 mm × 0.5 mm.

CNT Growth: The nanotubes (diameter ~80 nm) were grown from the Ni catalyst at 700°C, using a C_2H_2 and NH_3 gas mixture. The growth pressure was 4 mbar (1 mbar = 100 Pa), which led to a growth rate of 0.2 μm min^{-1}. A detail description of MWCNT growth by this technique can be found elsewhere [28].

WILEY InterScience® DISCOVER SOMETHING GREAT
© 2009 WILEY-VCH Verlag GmbH & Co. KGaA, Weinheim

Amorphous-Silicon Deposition: The following conditions were used: substrate temperature 250°C; deposition pressure 350 mbar; SiH_4:H_2 ratio 10%; radio-frequency power 70 mW cm^{-2}; PH_3:SiH_4 ratio 0.5%.

Solar-cell Characterization: The current–voltage characteristics were measured using a HP 4140B sourcemeter. For white-light efficiency measurement (at 100 m Wcm^{-2}), an Oriel solar simulator (Model 96000) with an AM 1.5 G filter was used. The light intensity was measured by a Newport-calibrated solar cell. The apparent current density (J_{sc}) is calculated by dividing the measured current by the actual tungsten contact area (0.5 mm × 0.5 mm). The saturation current, I_0, and the diode ideality factor, N, were extrapolated from the ideal diode equation: $\ln(I) = \frac{q}{NkT}V + \ln(I_0)$

Coaxial Capacitance Calculation: The capacitance of a single coaxial solar-cell structure was approximated by a cylindrical capacitor model $C = 2\pi\varepsilon_0\varepsilon_r l/\ln(b/a)$, [20] where ε_0 is permittivity in a vacuum, ε_r is the dielectric constant of a-Si:H, l is nanotube length, a is nanotube diameter, and b is the coaxial diameter of a-Si:H. Using this model with $\varepsilon_0 = 8.85 \times 10^{-14}$ Fcm^{-1}, $\varepsilon_r = 11.7$, $l = 2.5\mu m$, $a = 80$ nm and $b = 580$ nm, the capacitance of one coaxial structure is calculated to be 0.812 fF. In device PV-1, each row of CNTs is 478 μm; assuming the diameter of each coaxial CNT–amorphous-silicon–ITO column is 640 nm and all such columns are closely packed in the row, there will be approximately 750 coaxial columns in each row, with 239 rows, giving a total number of coaxial columns of 179 250. The total capacitance calculated according to the above formula is 146.16 pF, which is in good agreement with the value measured (125 pF) at 100 kHz.

Acknowledgements

Support from the CU Centre for Advanced Photonics and Electronics (CAPE) under the Strategic Research initiative is gratefully acknowledged. We thank Dr. E. Unalan for discussion on the low-dimensional material and S. C. Tan for advice on the External Quantum Efficiency measurements. Prof. J. I. B. Wilson from Heriot-Watt University and Prof. X. Lin from Shantou University are also thanked for helpful discussions on amorphous-silicon solar cells. This article is part of the Special Issue celebrating the 800th Anniversary of Cambridge.

Received: March 31, 2009
Revised: May 15, 2009
Published online: August 17, 2009

[1] N. S. Lewis, *Science* **2007**, *315*, 798.
[2] D. Kuang, J. Brillet, P. Chen, M. Takata, S. Uchida, H. Miura, K. Sumioka, S. M. Zakeeruddin, M. Gratzel, *ACS Nano* **2008**, *2*, 1113.
[3] M. Law, L. E. Greene, J. C. Johnson, R. Saykally, P. Yang, *Nat. Mater.* **2005**, *4*, 455.
[4] W. U. Huynh, J. J. Dittmer, A. P. Alivisatos, *Science* **2002**, *295*, 2425.
[5] E. Kymakis, G. A. J. Amaratunga, *Appl. Phys. Lett.* **2002**, *80*, 112.
[6] J. B. Baxter, E. S. Aydil, *Appl. Phys. Lett.* **2005**, *86*, 053114.
[7] J. Y. Kim, K. Lee, N. E. Coates, D. Moses, T.-Q. Nguyen, M. Dante, A. J. Heeger, *Science* **2007**, *317*, 222.
[8] B. M. Kayes, H. A. Atwater, N. S. Lewis, *J. Appl. Phys.* **2005**, *97*, 114302.
[9] L. Hu, G. Chen, *Nano Lett.* **2007**, *7*, 3249.
[10] B. Tian, X. Zheng, T. J. Kempa, Y. Fang, N. Yu, G. Yu, J. Huang, C. M. Lieber, *Nature* **2007**, *449*, 885.
[11] X. Wang, J. Song, J. Liu, Z. L. Wang, *Science* **2007**, *316*, 102.
[12] Y. Zhang, L. W. Wang, A. Mascarenhas, *Nano Lett.* **2007**, *7*, 1264.
[13] M. A. Green, *Solar Energy* **2003**, *74*, 181.
[14] L. Tsakalakos, J. Balch, J. Fronheiser, B. A. Korevaar, O. Sulima, J. Rand, *Appl. Phys. Lett.* **2007**, *91*, 233117.
[15] K. Q. Peng, Y. Xu, Y. Wu, Y. J. Yan, S. T. Lee, J. Zhu, *Small* **2005**, *1*, 1062.
[16] M. D. Kelzenberg, D. B. Turner-Evans, B. M. Kayes, M. A. Filler, M. C. Putnam, N. S. Lewis, H. A. Atwater, *Nano Lett.* **2008**, *8*, 710.
[17] S. Frank, P. Poncharal, Z. L. Wang, W. A. Heer, *Science* **1998**, *280*, 1744.
[18] E. Yablonovitch, *Phys. Rev. Lett.* **1987**, *58*, 2059.
[19] R. Camacho, A. Morgan, M. Flores, T. McLeod, V. Kumsomboone, B. Mordecai, R. Bhattacharjea, W. Tong, B. Wagner, J. Flicker, S. Turano, W. Ready, *J. Miner. Met. Mater. Soc.* **2007**, *59*, 39.
[20] J. E. Jang, S. N. Cha, Y. J. Choi, D. J. Kang, T. P. Butler, D. G. Hasko, J. E. Jung, J. M. Kim, G. A. J. Amaratunga, *Nat. Nanotechnol.* **2008**, *3*, 26.
[21] V. T. Daudrix, J. Guillet, F. Freitas, A. Shah, C. Ballif, P. Winkler, M. Ferreloc, S. Benagli, X. Niquille, D. Fischer, R. Morf, *Prog. Photovolt: Res. Appl.* **2006**, *14*, 485.
[22] O. Vetterl, F. Finger, R. Carius, P. Hapke, L. Houben, O. Kluth, A. Lambertz, A. Mück, B. Rech, H. Wagner, *Sol. Energy Mater.* **2000**, *62*, 97.
[23] D. L. Staebler, C. R. Wronski, *J. Appl. Phys.* **1980**, *51*, 3262.
[24] A. Kolodziej, *Opto-Electronics Rev.* **2004**, 12.
[25] Z. F. Ren, Z. P. Huang, D. Z. Wang, J. G. Wen, J. W. Xu, J. H. Wang, L. E. Calvet, J. Chen, J. F. Klemic, M. A. Reed, *Appl. Phys. Lett.* **1999**, *75*, 1086.
[26] K. B. K. Teo, M. Chhowalla, G. A. J. Amaratunga, W. I. Milne, D. G. Hasko, G. Pirio, P. Legagneux, F. Wyczisk, D. Pribat, *Appl. Phys. Lett.* **2001**, *79*, 1534.
[27] T. D. Wilkinson, X. Wang, K. B. K. Teo, W. I. Milne, *Adv. Mater.* **2008**, *20*, 363.
[28] M. Chhowalla, K. B. K. Teo, C. Ducati, N. L. Rupesinghe, G. A. J. Amaratunga, A. C. Ferrari, D. Roy, J. Robertson, W. I. Milne, *J. Appl. Phys.* **2001**, *90*, 5308.

© 2009 WILEY-VCH Verlag GmbH & Co. KGaA, Weinheim